INFRARED TEMPERATURE MAPPING IN ELASTOHYDRODYNAMIC LUBRICATION

A THESIS

Presented to

The Faculty of the Division of Graduate

Studies and Research

By

Vernon Knox Ausherman, Jr.

In Partial Fulfillment

of the Requirements for the Degree

Master of Science

in Mechanical Engineering

Georgia Institute of Technology

March 1975

INFRARED TEMPERATURE MAPPING

IN ELASTOHYDRODYNAMIC LUBRICATION

Approved:

David M. Sanborn, Chairman

Ward O. Winer

J. T. Berry

John L. Lundberg

Date approved by Chairman: 2-26-75

ACKNOWLEDGMENTS

The author wishes to express his gratitude to his reading committee for their time and interest. Guidance and suggestions given by Dr. David M. Sanborn, the committee chairman, and Dr. Ward O. Winer are particularly appreciated.

The research presented here was funded in part by NASA (NGR-11-002-133) and the National Science Foundation (GK-31154).

In addition, the author would like to acknowledge the assistance of H. S. Nagaraj, who was of great help in all aspects of this research.

TABLE OF CONTENTS

LIST OF ILLUSTRATIONS

NOMENCLATURE

A, B, C, D, E, F	Calibration constants
A', B', C', D', E', F'	Calibration constants
A_1, A_2	Calibration constants
B_1, B_2	Calibration constants
h	Film thickness
N	Total radiation intensity measured at some location in the contact
N_a	Unreferenced filter calibration radiation intensity
$N_{a(amb)}$	Ambient reference radiation intensity
N_b	Nonattenuated ball radiation intensity
N_{bb}	Radiation intensity from a blackbody source
n_{bb}	Monochromatic radiation intensity from a blackbody source
N_f	Nonattenuated fluid (lubricant) radiation intensity
n_f	Total monochromatic radiation intensity from the fluid
n_f^*	Monochromatic fluid radiation intensity, neglecting reflected component
N_{fil}	Intensity of radiation emitted by filter
n_{fr}	Monochromatic radiation intensity from the reflected fluid component
N_i	Intensity of radiation entering the fluid from an arbitrary source
n_i	Monochromatic radiation intensity entering the fluid from an arbitrary source

N_m	Measured calibration radiation intensity
N_o	Nonattenuated ambient radiation intensity
N_o'	Detector reference constant
N_s	Nonattenuated sapphire radiation intensity
N_t	Intensity of radiation from an arbitrary source transmitted through the fluid
n_t	Intensity of monochromatic radiation from an arbitrary source transmitted through the fluid
N_1, N_2, N_3	Constants for calibration least squares data fitting
T	Temperature
T_b	Ball surface temperature
T_c	Calibration temperature
T_f	Fluid (lubricant) average temperature
T_r	Room temperature
α_1, α_2, α_3	Fluid absorption coefficients
α^*	Monochromatic fluid absorption coefficient
ϵ_b	Ball emissivity
ϵ_f	Fluid emissivity
ϵ_1, ϵ_2, ϵ_3	Fluid emissivity coefficients
η_b	Attenuation factor for ball radiation
η_f	Attenuation factor for fluid radiation
η_o	Attenuation factor for ambient radiation
η_s	Attenuation factor for sapphire radiation
λ	Wavelength
ρ_a	Attenuation due to Fresnel reflection losses at the sapphire-air interface
ρ_b	Ball reflectivity

ρ_f	Attenuation factor due to Fresnel reflection losses at the sapphire-lubricant interface
ρ_s^*	Sapphire total reflectance
τ^*	Monochromatic lubricant transmissivity
τ_f	Lubricant transmissivity
τ_s	Sapphire transmissivity
τ_s^*	Sapphire total transmittance

SUMMARY

This research is concerned with the development of an experimental method to measure the temperature of bearing elements and lubricants in elastrohydrodynamic (EHD) sliding point contacts. The EHD contact used in the experimental work is designed to be representative of conditions found in the lubrication of many cams, gears, and bearings where relative surface motion is encountered between lubricated, load-supporting surfaces. Because very little is known about either the magnitude or the variation of temperatures under these conditions, a reliable technique capable of measuring temperatures at locations of interest could be of significant value to designers.

The experimental apparatus used in this work forms an EHD contact by rotating a chrome steel ball loaded against a sapphire disk. Infrared radiation from the heat generating region is transmitted through the sapphire and collected by an infrared microdetector. This research presents a technique whereby the measured values of radiation intensity at various locations in the contact can be reduced to yield temperatures for both the lubricant and the ball surface. Calculation of the individual temperatures is made possible by taking separate measurements at the same location through different infrared filters attached to the microdetector.

To complement the main analysis and to show the feasibility of this method, a presentation of data obtained using the technique is included.

CHAPTER I

INTRODUCTION

The objective of this research is to develop and refine a technique to measure temperatures of bearing element surfaces and test fluids in elastohydrodynamic sliding point contacts. Elastohydrodynamic (EHD) lubrication is concerned with the study of bearings in which elastic deformation of the machine elements has a significant influence on the hydrodynamic lubrication process. These conditions are frequently encountered in several lubrication situations, including the lubrication of ball bearings, roller bearings, cams, and gears. In each of these cases, a load between two nonconforming machine elements is carried over a contact area which is often referred to as being either a point or line. This is due to the fact that its size is orders of magnitude smaller than an equivalent radius of curvature of the machine elements.

An adequate understanding of the EHD lubrication process requires an understanding of both hydrodynamic and boundary lubrication. Under ideal conditions the bearing surfaces are separated by a continuous lubricant film created by the classical hydrodynamic lubrication mechanism, and the bearing operates outside of the boundary lubrication (surface contact) regime, resulting in less wear. Nevertheless, the bearing elements are subjected to extremely large cyclic stresses which can cause fatigue failure as well as additional stress or wear wherever the heights of surface asperities are of the same

order as the lubricant film thickness. As a consequence, designers of EHD bearings cannot always assume an infinite bearing life as is often the case for hydrodynamic bearings. Due to these considerations, many EHD bearings are also designed to operate under boundary lubrication conditions for extended periods of time, while hydrodynamic bearings, as a rule, are not.

The load carried per unit bearing area is much larger in an elastohydrodynamic bearing than in hydrodynamic bearings. Theory predicts that the load per unit bearing area will, in many cases, closely resemble the Hertzian pressure distribution that would be formed if unlubricated surfaces were placed in static contact under the same normal load and allowed to elastically deform [1]. Hertzian pressures for some bearings reach as high as 2.8×10^9 N/m^2 and the actual pressure may be even higher in places. In addition to these high contact pressures, the lubricant film is very thin, usually anywhere from 3×10^{-8} to 4×10^{-7} m in the load-supporting region [2]. The lubricant films are thin enough to be of the same order of height as the surface asperities themselves. Asperity interactions cause added wear and friction which is generally thought to be a result of direct contact. However, it has been suggested that there is also lubrication between individual asperities [3], causing them to deform either elastically or plastically without actual surface contact.

The severe operating conditions described above cause marked changes in fluid properties. In addition to the large pressures, a typical fluid element in the contact is subjected to shear stresses as high as 7×10^7 N/m^2 and shear rates as high as 10^7 sec^{-1}. This large

rate of energy input per unit fluid volume due to mechanical shearing is not encountered in conventional hydrodynamic lubrication situations and most lubricants are not selected on the basis of these criteria.

The subject of fluid behavior in EHD contacts has been the subject of several investigations of both an analytical and an experimental nature. Analytical investigations usually consist of a numerical iteration to solve for parameters of interest throughout the bearing contact area. These parameters include pressure, temperature, density, and viscosity. Most of these iterations are based on the Reynolds equation, an elasticity equation for the bearing surfaces, and a formulation describing the fluid viscosity. When sliding contacts are considered, the energy equation as well as a temperature dependent viscosity model must be included. In addition to providing values for parameters such as pressure and temperature, these iterations can provide values for film thickness and traction which can then be compared to experimental data. Some treatments of this nature are given by Cheng and Sternlicht [4], Crook [5], and Dowson and Higginson [6].

Although analytical examinations of the EHD problem have been conducted with considerable depth and complexity, they have been unable to consistently predict experimental results, particularly in the case of traction measurements. Furthermore, even if the experimental and analytical work were in better agreement, there would still not be any assurance that the predicted temperatures, pressures, and viscosities are also correct. This situation is caused in part by a lack of data for temperatures and pressures in the contact to supplement traction

and film thickness data. Therefore, most of the available information concerning temperature and pressure conditions in the contact is a result of analytical rather than experimental work.

Viscosity is perhaps the most important lubricant property due to its affect on both film thickness and traction. Lubricant viscosities are well known under standard or near ambient conditions, but their large variations with temperature and pressure in EHD environments make them very difficult to predict. Jakobsen [7] has measured viscosities at shear stresses as high as 4.8×10^6 N/m^2, but this is still an order of magnitude below the shear stresses encountered in an EHD contact. Even though his work found that the base lubricants were Newtonian at these high shear stresses, there is good reason to believe that the fluid exhibits non-Newtonian behavior when subjected to the mechanical shearing evident in some cases. Experimental work by Walker [8] showed that lubricants containing high molecular weight polymers can undergo substantial molecular degradation in a single passage through a sliding contact. This could indicate a serious loss of viscosity that would not be anticipated by most viscosity models found in the literature. Because viscometry has not yet advanced to the point where EHD conditions can be artificially simulated in order to determine their exact influences on viscosity, these effects must be measured in actual EHD contacts.

Based on the current state of experimental data available in elastohydrodynamic lubrication, a method to experimentally measure pressure or temperature at various locations in a bearing contact area under different conditions would probably be of great value in bearing

analysis and design. Theoretical treatments show better agreement for pressure than for temperature despite the fact that pressure has never been experimentally mapped through the contact. EHD theory predicts that the contact pressure distribution will in many cases follow a nearly Hertzian pressure profile except for a sharp peak near the exit. Even if the actual values are not well known as functions of position, pressures of the proper magnitude can be determined by simply comparing the bearing load with the size of the contact area.

Temperature, on the other hand, is more difficult to predict due to the complicated energy balance which must be considered. As was previously mentioned, analytical temperature mapping involves the simultaneous numerical solution of a number of equations describing the lubricant and the bearing surfaces. Because of the large number of unknowns in analyses such as these, any errors in the analysis would probably cause errors of an unknown magnitude in the calculated temperatures. As a result, these techniques cannot be expected to provide accurate and reliable information about temperatures, and direct experimental observations could be of considerable value.

Experimental fluid temperature data would also contribute significantly to a better understanding of the energy dissipation mechanisms in the contact. Some energy added to the fluid by mechanical shearing is removed by conduction and convection while other energy induces molecular degradation of the lubricant [8]. Temperature data would help to determine the relative contributions of these processes and give some indication of changes in the basic fluid heat transfer characteristics under extreme conditions. High temperatures would

also locate sources of excessively high energy input which might signal some form of film breakdown.

An infrared radiation temperature mapping technique has been developed through this research which can map temperatures both in the lubricant and at a bearing surface in an EHD sliding point contact. Radiation at any location is collected and measured by a radiometric microscope focused on that location. Any measurement of this nature will consist of combined radiation from both bearing surfaces as well as the lubricant. Techniques have been devised to determine the values of radiation emitted by the various sources and, as a result, obtain the temperatures of these sources. This method has two distinct advantages over ordinary measurements taken by inserting transducers into the contact: (1) thermocouples and other transducers are simply too large to fit into the contact, and (2) the microdetector used in this research can focus on a spot 3.8×10^{-5} m in diameter while most transducers do not have comparable resolution.

The first such approach to this problem was carried out in this laboratory and is described by Turchina [9] and Turchina, Sanborn, and Winer [10]. This work was used as a basis for the treatment given here.

CHAPTER II

DESCRIPTION OF TEST APPARATUS

The test apparatus used in this research is basically the same one that has been used extensively in previous studies [2, 8, 9, 10, 11], and is shown in Figure II-1. An EHD sliding point contact is created inside the test rig by rotating a 0.0318 in diameter chrome steel ball (AISI 52100, composition: 1% C, 1-1/2% Cr) loaded against a synthetic sapphire disk, 0.0016 m thick. Both surfaces have a surface roughness of approximately 3×10^{-8} m (1 microinch) rms. The ball is rotated by a variable speed dc motor which can provide any ball surface speed in the desired range. The sapphire is supported by a pivoted assembly and is located directly above the ball. The contact is loaded by adding weight to the assembly, causing the sapphire to be forced downward against the ball.

The lubricant being investigated is a naphthenic mineral oil supplied by the Sun Oil Company. The lubricant's atmospheric pressure viscosity is 0.0217 Ns/m^2 (21.7 cp) at 37.8°C and 0.0032 Ns/m^2 (3.2 cp) at 98.9°C. Detailed information concerning the test fluid can be found in References [2] and [11].

The ball is almost totally immersed in the contact feed reservoir and oil is drawn up into the contact by viscous action due to the ball's rotation (see Figure II-1). Care must be taken at high speeds to insure that enough lubricant is drawn into the contact area to prevent starvation of the oil supply. Oil is supplied by an oil

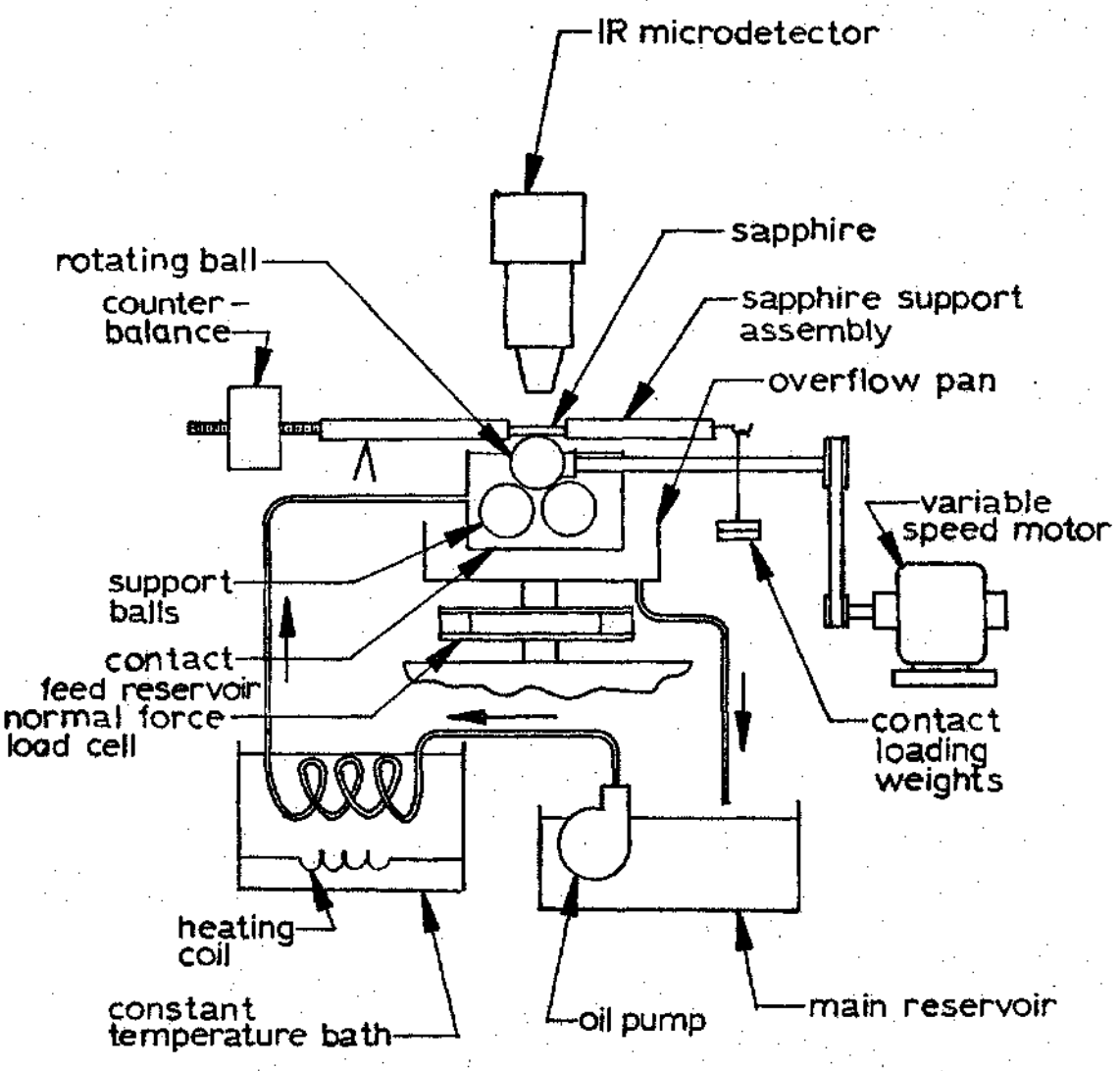

Figure II-1. Test Apparatus

circulation system in which the test lubricant is pumped through a constant temperature bath and into the bottom of the contact feed reservoir, causing it to spill over the sides and into an overflow pan. From there it drains back into the main reservoir. The purpose of the constant temperature bath is to keep the oil in the contact feed reservoir at a constant temperature for all experiments. The lubricant temperature is monitored by a thermocouple in the contact feed reservoir and can be varied by controlling the power supplied to the heating coil in the constant temperature bath.

The oil circulation system and the loading mechanism were both designed for application in this research. Previously, the EHD contact was found to add enough energy to the test lubricant to raise the temperature in the contact feed reservoir by over 20°C. The new loading mechanism was built in the interest of obtaining a loading force closer to the normal.

IR radiation from the contact is measured by a Barnes Model RM-2A In-Sb Microdetector mounted directly above the sapphire. The microdetector is mounted on a movable suspension which can be driven at constant speeds as low as 4.8×10^{-5} m/sec, allowing the detector to transverse the contact during test runs. The microdetector contains an optical system which permits focusing on any spot in the contact with a resolution of 3.8×10^{-5} m diameter. This resolution is satisfactory in this application since the bearing contact area is 0.0038 m in diameter, or 100 times larger.

The output of the detector is amplified and displayed on an oscilloscope. As the microdetector moves across the contact, a trace

is made on the oscilloscope which is then photographed. The resulting picture provides a continuous plot of radiation intensity versus distance traveled across the contact. By running several such traverses, a complete map can be drawn showing IR radiation levels for each point in the contact plane.

CHAPTER III

ANALYSIS FOR DETERMINATION OF CONTACT TEMPERATURES

Basic Approach

Figure III-1 shows the various sources which emit the radiation received by the detector from an arbitrary spot in the contact. The radiation consists of contributions from the ball (N_b), fluid (N_f), sapphire (N_s), and ambient (N_o). The variables N_b, N_f, N_s, and N_o refer to nonattenuated radiation from the various sources, or the radiation which would be measured if the source could be observed separately. The term "ambient" refers to background radiation from the room which reflects off of the spot and into the detector. The fluid and sapphire are both semi-transparent media and will partially absorb IR radiation passing through them. In addition, the total quantity of radiation will be affected by Fresnel reflection losses at each interface between different media. These attenuations are represented by the attenuation factors η_b, η_f, η_s, and η_o which can be defined simply as the ratio of the radiation from a particular source reaching the detector to the radiation that would reach the detector without attenuation. The total radiation collected by the detector, N, then is given by equation (1).

$$N = \eta_b N_b + \eta_f N_f + \eta_s N_s + \eta_o N_o \qquad (1)$$

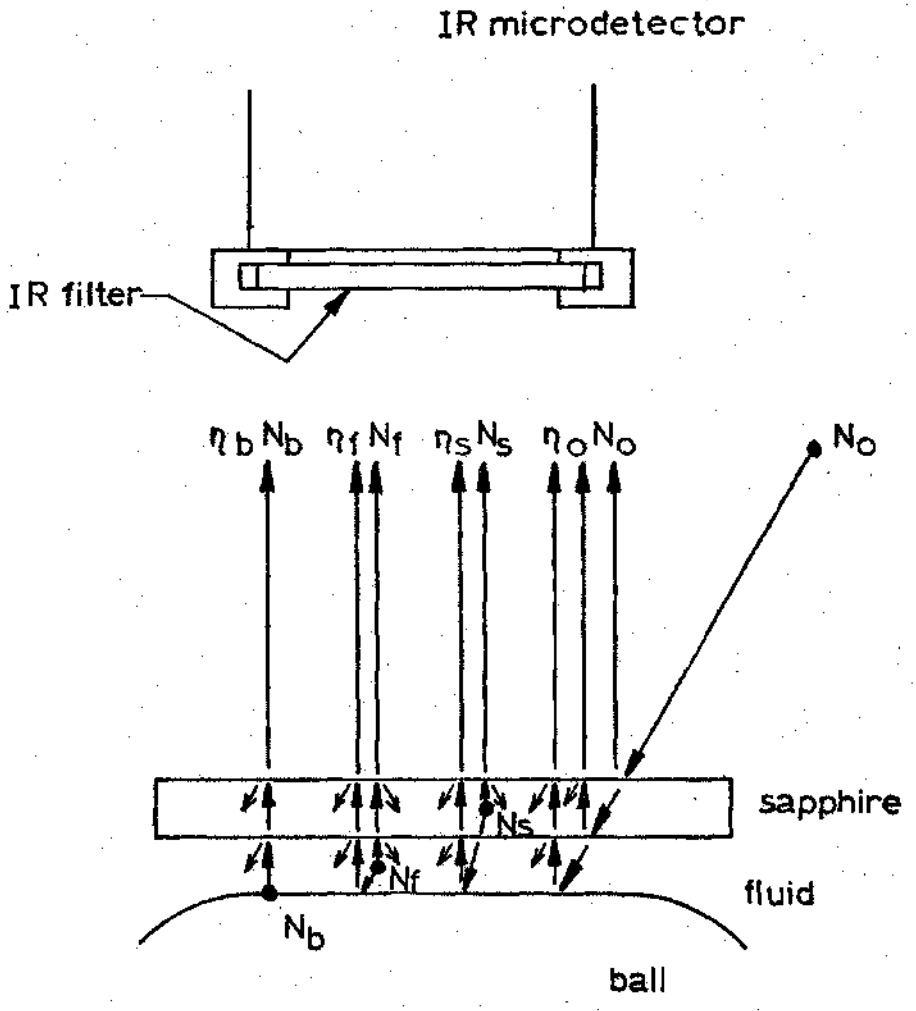

Figure III-1. Sources of IR Radiation Emitted from An Arbitrary Location in the Contact

Determination of the temperature of either the fluid, ball, or sapphire requires that the emission and transmission characteristics of each medium be known.

Due to the complexity of the problem, it is impossible to determine the individual values of N_b, N_f, and N_s by making a single measurement with the detector. However, by making two measurements at each point of interest and by taking into account the variation in spectral emission characteristics of the different sources, values for N_b and N_f can be obtained. The temperatures of the ball surface and the fluid can then be determined, provided that emissive properties of the sources are known. At present, the sapphire temperature cannot be separated and calculated independently, but variations in sapphire radiation due to changing temperatures have been accounted for by making certain assumptions, to be discussed below.

The two measurements are taken under identical conditions except that a different IR filter has been mounted on the detector in each case. One filter was selected in order to accentuate the fluid contribution, the other to eliminate it. These filters were chosen by considering data of the test lubricant's spectral characteristics, plotted in Figure III-2, which show the monochromatic absorptivity of a 2.5×10^{-5} m (.001 inch) thick oil film as a function of wavelength. The results show that the oil is highly absorbent in the spectral range from 3.1 to 3.7 microns. Therefore, assuming that monochromatic emissivity is equal to monochromatic absorptivity [12], the oil also must be a strong emitter of radiation in this band. In order to accentuate this emission band, a filter was selected which only

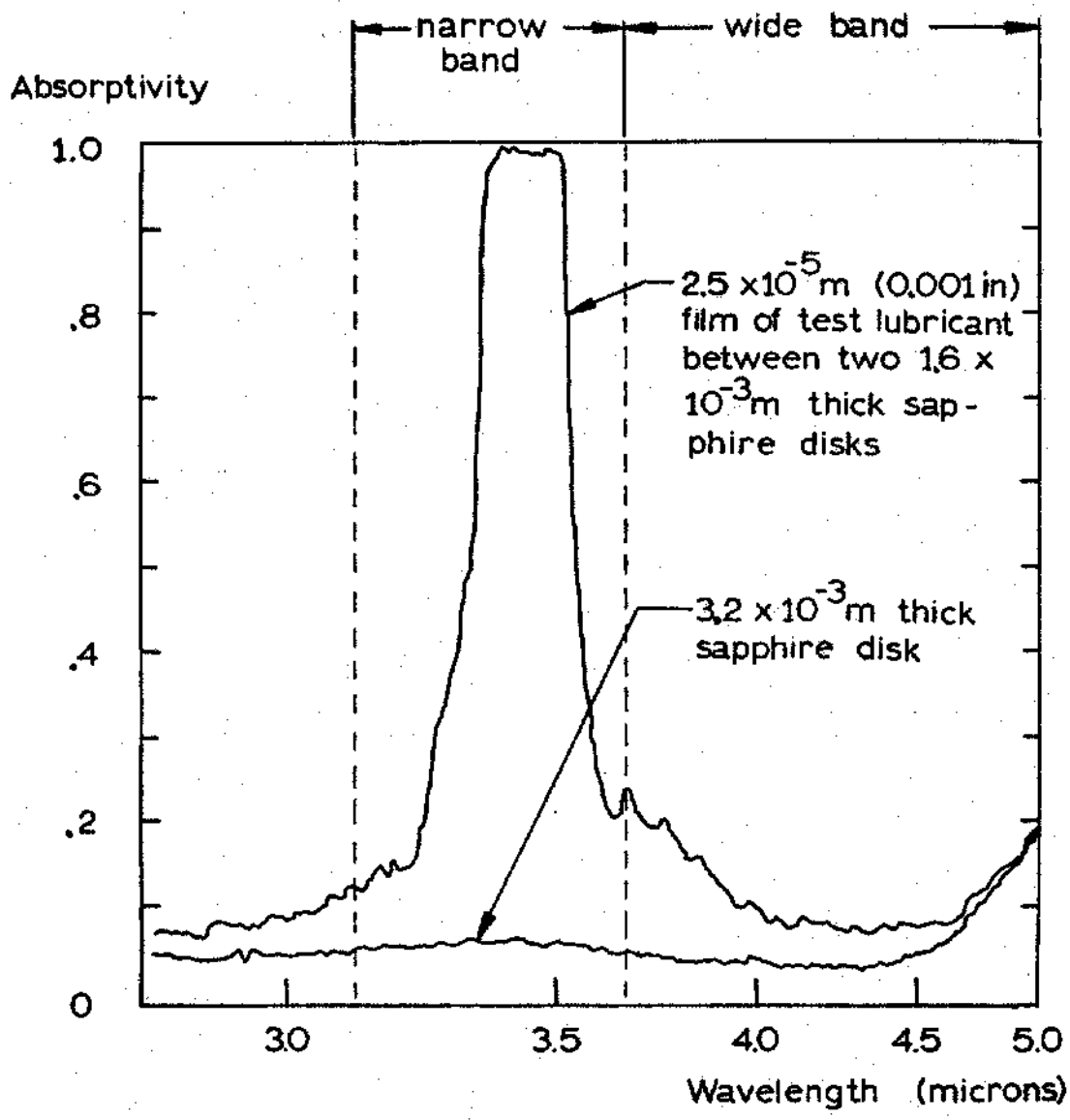

Figure III-2. Test Lubricant Absorptivity

transmits radiation between 3.1 and 3.7 microns, and which will be referred to as the narrow band filter. The spectral data also show that there is very little absorption of radiation between 3.7 and 5.0 microns by a 2.5×10^{-5} m oil film. Likewise, any absorption or emission from a film of EHD thickness should also be very small since an EHD film is much thinner than 2.5×10^{-5} m. This is due to the fact that absorption of radiation at any wavelength is an inverse exponential function of film thickness and, as a result, thick fluid films are more absorptive than thin ones. Accordingly, another filter was selected which transmits radiation in the spectral range from 3.7 to 5.0 microns, and which will be referred to as the wide band filter.

When a filter is used in the experiment, the problem becomes more complex because the filter will further attenuate the total radiation given in equation (1). This attenuation is unknown and in general will be different for each source of radiation. The increased complexity is remedied somewhat by simply assuming that the filter is part of the detector and combining the filter response with the detector response. It must be remembered that, when using the filters, the calibration curves supplied for the detector are no longer applicable, and the detector must be recalibrated for each filter and each radiation source.

Wide Band Filter Analysis

The wide band filter analysis is designed to provide the ball surface temperature by making a single measurement. This is possible because the filter does not transmit any radiation emitted by the fluid and variations in fluid temperature do not directly affect the

total radiation received by the detector. Since the fluid does not radiate in this band, equation (1) can be rewritten without the fluid term.

$$N = \eta_b N_b + \eta_s N_s + \eta_o N_o \tag{2}$$

It should be mentioned at this point that these are the same variables that will be used later in the narrow band filter analysis, but that any equations given in the wide band section do not necessarily apply for the narrow band and vice versa. The total nonattenuated ball radiation, N_b, can be calculated by equation (3).

$$N_b = \varepsilon_b N_{bb}(T_b) \tag{3}$$

The variable ε_b represents the ball emissivity and T_b is the ball surface temperature. The emissivity was measured in a separate experiment using the microdetector, and is assumed to remain constant for all temperatures. Metallic surfaces of this nature are often assumed to be grey bodies; that is, their emissivity is independent of both wavelength and temperature [13]. The emissivity was measured by performing calibration experiments using both filters and using no filter at all. The filter selection had no discernible effect on emissivity, indicating that the ball surface closely resembles a grey body. The radiation that would be observed through the filter from a blackbody at temperature T is referred to as $N_{bb}(T)$. By taking measurements of the radiation observed through the filter of a blackbody at various temperatures, a plot of $N_{bb}(T)$ versus T has been obtained.*

*See Chapter IV of thesis.

The ball radiation attenuation, η_b, is only dependent on the optical properties of the sapphire, since the fluid absorbs little in the 3.7 to 5.0 μ band. The attenuation of any radiation going through the sapphire is defined here as the total transmittance of the sapphire, τ_s^*, and can be written as follows:

$$\tau_s^* = \tau_s(1 - \rho_a)(1 - \rho_f) \tag{4}$$

The variable τ_s represents the sapphire transmissivity and ρ_a and ρ_f represent the Fresnel reflection losses at the sapphire-air and sapphire-fluid interfaces, respectively. The transmissivity, as opposed to the total transmittance, does not include reflection losses and is only dependent on the absorption losses in the sapphire. Transmissivity varies somewhat with wavelength in the infrared spectrum, and slightly different values have to be used for the two filters. The Fresnel reflection losses occur at any interface between media of different refractive indices and are independent of wavelength. In view of the fact that the largest Fresnel reflection loss is only 0.07 between any two media, secondary reflections can be neglected.

The intensity of incident ambient radiation, N_o, is equal to the intensity of radiation emitted from a blackbody at room temperature, and is known from calibration.* Some of the ambient radiation will be reflected directly by the sapphire before reaching the fluid. This attenuation is defined as the sapphire total reflectance, ρ_s^*, and depends on both transmissivity and Fresnel losses as does the

---

*See Chapter IV of thesis.

total transmittance. The total reflectance can be expressed by equation (5).

$$\rho_s^* = \rho_a + \tau_s^2 (1 - \rho_a)^2 \rho_f \tag{5}$$

In addition, some of the ambient radiation is transmitted through the sapphire, reflected off the ball surface, and transmitted back through the sapphire. Adding this contribution to that which is reflected directly from the sapphire yields the total ambient attenuation.

$$\eta_o = \rho_s^* + \rho_b \tau_s^{*2} \tag{6}$$

The ball reflectivity, ρ_b, is equal to one minus the emissivity, since the ball is opaque.

The sapphire contribution is considerably harder to analyze than the other radiation sources because its temperature varies from an EHD contact temperature at the fluid boundary to a nearly ambient temperature at the other surface. Furthermore, the sapphire, unlike the fluid, radiates at all wavelengths that can be measured by the detector and sapphire radiation cannot be separated from ball radiation by measuring through different filters. These circumstances make it impossible at this time to either measure radiation emitted by the sapphire or solve for the sapphire temperature. Nevertheless, it would seem likely that the sapphire contribution could be neglected for two reasons: (1) the sapphire emissivity has been shown to be roughly 10 times smaller than the ball emissivity, based on absorption data; and (2) the average temperature of the sapphire is expected to be a great deal lower than the ball surface temperature. If the

sapphire radiation is neglected, equations (3) and (6) can be substituted into equation (2) and written as equation (7).

$$N = \tau_s^* \varepsilon_b N_{bb}(T_b) + (\rho_s^* + \tau_s^{*2}\rho_b)N_o \tag{7}$$

Once a value of N has been obtained experimentally, the only unknown in equation (7) is the ball temperature, T_b.

To reduce radiation intensities to ball temperatures, equation (7) is first solved for $N_{bb}(T_b)$.

$$N_{bb}(T_b) = \frac{(\rho_s^* + \tau_s^{*2}\rho_b)N_o}{\tau_s^*\varepsilon_b} \tag{8}$$

After solving for N_{bb}, T_b can be obtained either by referring to calibration data, or by using Figure III-3, which shows a plot of the detector output versus the ball surface temperature. Figure III-3 was obtained by substituting calibration data into equation (8). Equation (9) is a least squares curve fit to Figure III-3 which allows calculation of ball surface temperatures directly from test data.

The above analysis was verified by taking measurements through the wide filter of a stationary ball in a circulating oil bath at a known temperature.* In these measurements, the film thickness was representative of values encountered in EHD situations and the circulating bath insured that the ball and fluid were both at the same temperature. The trial measurements showed that variations in film

---

*This is the same basic experimental setup as is used for the fluid calibration and is explained in Chapter IV.

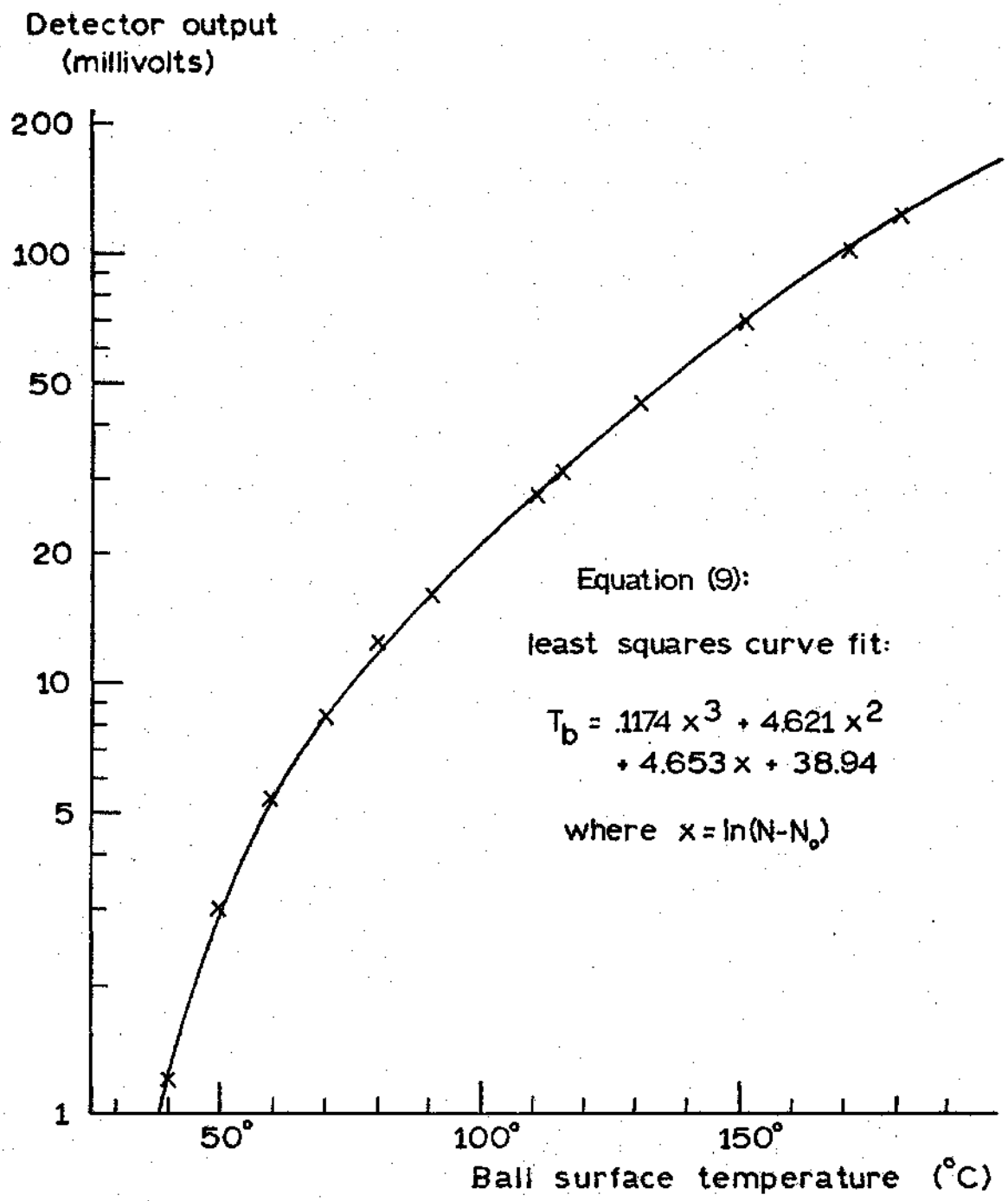

Figure III-3. Detector Output versus Ball Surface Temperature

thickness had no discernible effect on the total radiation intensity and that calculated ball temperatures were consistently within 2°C of the bath temperature as measured by a thermocouple. These test results tend to substantiate the wide band analysis as a whole and, in particular, the elimination of the sapphire contribution. The reason for this has to do with the relative sapphire contribution in the test run. In the test the sapphire, ball, and fluid were all at the same temperature, but under EHD conditions the average sapphire temperature would be expected to be lower than that of either the fluid or the ball surface. Therefore, any error caused by neglecting the sapphire would probably be larger in the test run than under actual experimental conditions.

Narrow Band Filter Analysis

The narrow band filter analysis is considerably more complicated than that of the wide band filter, due to emission and absorption by the oil. The total fluid radiation which would be observed without attenuation due to the sapphire is defined as follows:

$$N_f = \epsilon_f(h, T_f, \rho_b) N_{bb}(T_f) \qquad (10)^*$$

The emissivity of a given lubricant, ϵ_f, is shown here as an unknown function of film thickness, fluid temperature, and the ball reflectivity. The blackbody radiation function, $N_{bb}(T)$, has the same meaning here as it did in the wide band filter analysis, but it will generally differ

*As was already mentioned, some of these terms are the same ones that were used in the wide band filter analysis, but they will have different values when used in narrow band filter calculations.

in value due to the difference in filters. There will also be some radiation included in N_f which is radiated downward, reflected off the ball, and then partially absorbed as it passes back through the fluid. Because the quantity of radiation which reflects off the ball depends on the ball reflectivity, the reflectivity must also be included in the fluid emissivity function. The emissivity is determined below.

The total radiation at wavelength λ which will be emitted at one boundary of a fluid film of thickness h and temperature T_f is defined as n_f^* and can be given by equation (11).

$$n_f^* = n_{bb}(\lambda,T_f)[1 - e^{-\alpha^*(\lambda,T_f)h}] \qquad (11)^*$$

The variable α^* is an absorption coefficient and the quantity $[1 - e^{-\alpha^*(\lambda,T_f)h}]$ is defined as the monochromatic emissivity. The small letter n is used to denote monochromatic radiation. The radiation that would be measured through the filter when focusing on a monochromatic blackbody source at temperature T and wavelength λ is written as $n_{bb}(\lambda,T)$. This equation is applicable for semitransparent emitting fluids at uniform temperature and in local thermodynamic equilibrium. The assumption of local thermodynamic equilibrium is a good one under these conditions, but the uniform temperature assumption is relatively poor since there are known to be appreciable changes in temperature over a distance of a few microinches. It should be remembered, however, that this technique is not capable of measuring temperatures at various locations across the film, and will give at best an

---

*This equation is derived in Reference [12].

average* temperature determined by accumulating radiation contributed from different fluid elements at different temperatures. On this basis, the absorption coefficient is considered as an "average" coefficient representative of the average temperature through the film.

The monochromatic transmissivity of the oil film, again assuming local thermodynamic equilibrium, will be equal to one minus the monochromatic emissivity.

$$\tau^* = 1 - [1 - e^{-\alpha^*(\lambda,T_f)h}]$$

$$= e^{-\alpha^*(\lambda,T_f)h} \qquad (12)$$

The quantity of monochromatic radiation reflected off the ball and transmitted back through the fluid, n_{fr}, is equal to the radiation emitted by the fluid film, n_f^*, multiplied by the ball reflectivity and the fluid transmissivity.

$$n_{fr} = n_f(\lambda,T_f,h)\rho_b\ \tau^*(\lambda,T_f,h)$$

$$= n_{bb}(\lambda,T_f)[1 - e^{-\alpha^*(\lambda,T_f)h}]\ \rho_b e^{-\alpha^*(\lambda,T_f)h} \qquad (13)$$

The total monochromatic radiation from the fluid, n_f, will then be the sum of n_f^* and n_{fr}.

---

*This average should not be thought of in the sense of an arithmetic mean. Because of the fourth power relationship between emitted radiation and temperature, the calculated temperature will be weighted toward the maximum temperature in the oil film.

$$n_f = n_f^*(\lambda,T_f,h) + n_{fr}(\lambda,T_f,h)$$

$$= n_{bb}(\lambda,T_f)[1 - e^{-\alpha^*(\lambda,T_f)h}]$$

$$+ \rho_b\, n_{bb}(\lambda,T_f)[1 - e^{-\alpha^*(\lambda,T_f)h}]e^{-\alpha^*(\lambda,T_f)h} \qquad (14)$$

Equation (14) can now be algebraically reduced.

$$n_f = n_{bb}(\lambda,T_f)[1 + (\rho_b - 1)e^{-\alpha^*(\lambda,T_f)h}$$

$$- \rho_b\, e^{-\alpha^*(\lambda,T_f)2h}] \qquad (15)$$

Using the series expansion for e^{-x} and retaining only the first four terms,* equation (15) can be reduced from its exponential form.

$$n_f = n_{bb}(\lambda,T_f)\{1 + (\rho_b-1)\{1 - \alpha^*(\lambda,T_f)h$$

$$+ \tfrac{1}{2!}[\alpha^*(\lambda,T_f)]^2 h^2 - \tfrac{1}{3!}[\alpha^*(\lambda,T_f)]^3 h^3\}$$

$$- \rho_b\{1 - \alpha^*(\lambda,T_f)(2h) + \tfrac{1}{2!}[\alpha^*(\lambda,T_f)]^2(2h)^2$$

$$- \tfrac{1}{3!}[\alpha^*(\lambda,T_f)]^3(2h)^3\}) \qquad (16)$$

Equation (16) can now be reduced and rewritten as equation (17).

---

*This assumption is justified because values of h are very small and $h^n/n!$ should rapidly approach zero as n becomes large.

$$n_f = n_{bb}(\lambda,T_f)\{(\rho_b + 1)h\ \alpha^*(\lambda,T_f) - \frac{1}{2}(3\rho_b + 1)h^2\ [\alpha^*(\lambda,T_f)]^2 + \frac{1}{6}(7\rho_b + 1)h^3\ [\alpha^*(\lambda,T_f)]^3\} \quad (17)$$

n_f is the combined monochromatic radiation at a particular wavelength which will leave the fluid and enter the sapphire. In order to determine the total fluid radiation entering the sapphire, N_f, the combined monochromatic radiation must be integrated over the narrow band filter spectrum.

$$N_f = \int_{3.1_\mu}^{3.7_\mu} n_f(\lambda,T_f,h)d\lambda$$

$$= (\rho_b + 1)h \int_{3.1_\mu}^{3.7_\mu} n_{bb}(\lambda,T_f)\alpha^*(\lambda,T_f)d\lambda - \frac{1}{2}(3\rho_b + 1)h^2 \int_{3.1_\mu}^{3.7_\mu} n_{bb}(\lambda,T_f)[\alpha^*(\lambda,T_f)]^2 d\lambda + \frac{1}{6}(7\rho_b + 1)h^3 \int_{3.1_\mu}^{3.7_\mu} n_{bb}(\lambda,T_f)[\alpha^*(\lambda,T_f)]^3 d\lambda \quad (18)$$

To integrate equation (18), the following coefficients of emissivity are defined.

$$\epsilon_1 = \frac{1}{N_{bb}(T_f)} \int_{3.1_\mu}^{3.7_\mu} n_{bb}(\lambda,T_f)[\alpha^*(\lambda,T_f)]d\lambda \quad (19a)$$

$$\varepsilon_2 = \frac{1}{2N_{bb}(T_f)} \int_{3.1_\mu}^{3.7_\mu} n_{bb}(\lambda,T_f)[\alpha^*(\lambda,T_f)]^2 d\lambda \qquad (19b)$$

$$\varepsilon_3 = \frac{1}{6N_{bb}(T_f)} \int_{3.1_\mu}^{3.7_\mu} n_{bb}(\lambda,T_f)[\alpha^*(\lambda,T_f)]^3 d\lambda \qquad (19c)$$

Using these coefficients, equation (18) is integrated and then simplified and written in the form of equation (20).

$$N_f = [(\rho_b + 1)h\varepsilon_1(T_f) - (3\rho_b + 1)h^2\varepsilon_2(T_f) + (7\rho_b + 1)h^3\varepsilon_3(T_f)]N_{bb}(T_f) \qquad (20)$$

When equation (20) is written in terms of the ball emissivity rather than reflectivity and combined with equation (10), equation (21) results.

$$\varepsilon_f(h,T_f)N_{bb}(T_f) = N_f = [(2 - \varepsilon_b)h\varepsilon_1(T_f) - (4 - 3\varepsilon_b)h^2\varepsilon_2(T_f) + (8 - 7\varepsilon_b)h^3\varepsilon_3(T_f)]N_{bb}(T_f) \qquad (21)$$

Equation (21) defines the fluid emissivity function $\varepsilon_f(h,T_f)$ in terms of the emissivity coefficients and is the basic fluid emission equation used in calibration and data reduction. It expresses the fluid emissivity coefficients ε_1, ε_2, and ε_3 as functions of the fluid temperature and relates them to the total radiation emitted by the fluid. Due to the fact that the absorption coefficient α^* is an

unknown function of fluid temperature, the emissivity coefficients are also unknown functions of temperature at this point. Since the fluid radiation only has to pass through the sapphire after leaving the fluid, the fluid attenuation, η_f, simply will be equal to the sapphire total transmittance.

$$\eta_f = \tau_s^* \tag{22}$$

The nonattenuated ball radiation can be given by the same equation that was used in the wide band analysis.

$$N_b = \varepsilon_b \, N_{bb}(T_b) \tag{3}$$

The attenuation factor η_b will be the same as for the wide band case, except that the fluid transmissivity, τ_f, must be included.

$$\eta_b = \tau_s^* \, \tau_f(T_f,h) \tag{23}$$

The fluid transmissivity function, τ_f, will be determined below.

The fluid transmissivity used for radiation from the ball is meant to apply to all grey or blackbody radiation passing through the fluid and is expressed in equation (23) as a generalized function of film thickness and fluid temperature. Based on Figure III-3, the oil is known to absorb radiation on a highly selective basis. Accordingly, the fluid transmissivity is also a function of the spectral characteristics of the incident radiation and, as a result, should also be a function of the temperature of the radiation source. However, all radiation which enters the fluid from other sources is assumed to be

blackbody in nature. This means that it will have been emitted from a grey body and that its spectral composition will correspond proportionately to the Planck blackbody function at some temperature. Since the Planck blackbody function is smooth in nature and the radiation being considered is only in a narrow band, temperature variations in the source should not appreciably affect the transmissivity for the radiation when it passes through the fluid, and such variations have been neglected. If the band were narrow enough to be considered monochromatic, the transmissivity would then be totally independent of the nature of the incident radiation.

Equation (12) is used to evaluate the fluid transmissivity function in terms of film thickness.

$$\tau^* = e^{-\alpha^*(\lambda,T_f)h} \tag{12}$$

Again using the exponential series expansion and retaining the first four terms, the monochromatic transmissivity is rewritten in the form of equation (24).

$$\tau^* = 1 - \alpha^*(\lambda,T_f)h + \frac{1}{2}[\alpha^*(\lambda,T_f)]^2h^2 - \frac{1}{6}[\alpha^*(\lambda,T_f)]^3h^3 \tag{24}$$

Now we consider monochromatic radiation entering the fluid from an arbitrary grey or blackbody source, referred to as n_i. The total radiation entering the fluid, N_i, is the integral of n_i over the narrow band.

$$N_i = \int_{3.1_\mu}^{3.7_\mu} n_i(\lambda)\,d\lambda \tag{25}$$

The monochromatic transmitted radiation, n_t, will be equal to the monochromatic incident radiation multiplied by the transmissivity function given in equation (24). The total transmitted radiation, N_t, can then be obtained by integrating over the narrow band.

$$N_t = \int_{3.1_\mu}^{3.7_\mu} n_t(\lambda, T_f, h)\,d\lambda$$

$$= \int_{3.1_\mu}^{3.7_\mu} n_i(\lambda)\{1 - \alpha^*(\lambda, T_f)h + \frac{1}{2}[\alpha^*(\lambda, T_f)]^2 h^2 - \frac{1}{6}[\alpha^*(\lambda, T_f)]^3 h^3\}\,d\lambda \tag{26}$$

To make integration possible, a set of absorptivity coefficients must be defined.

$$\alpha_1 = \frac{1}{N_i}\int_{3.1_\mu}^{3.7_\mu} n_i(\lambda)\alpha^*(\lambda, T_f)\,d\lambda \tag{27a}$$

$$\alpha_2 = \frac{1}{2N_i}\int_{3.1_\mu}^{3.7_\mu} n_i(\lambda)[\alpha^*(\lambda, T_f)]^2\,d\lambda \tag{27b}$$

$$\alpha_3 = \frac{1}{6N_i}\int_{3.1_\mu}^{3.7_\mu} n_i(\lambda)[\alpha^*(\lambda, T_f)]^3\,d\lambda \tag{27c}$$

The integrated transmitted radiation is then given by equation (28).

$$N_t = N_i\{1 - [\alpha_1(T_f)h - \alpha_2(T_f)h - \alpha_3(T_f)h^3]\} \tag{28}$$

Based on equation (28), a generalized fluid transmissivity can be obtained which is applicable to all grey or blackbody radiation passing through the oil film.

$$\tau_f = N_t/N_i$$

$$= 1 - [\alpha_1(T_f)h - \alpha_2(T_f)h^2 + \alpha_3(T_f)h^3] \tag{29}$$

The absorptivity coefficients α_1, α_2, and α_3 are similar to the emissivity coefficients previously defined in that they are unknown functions of the fluid temperature.

Radiation from the sapphire was neglected in the wide band analysis because it was significantly smaller than radiation from the ball. The sapphire would then be expected to likewise contribute a proportionately small amount of radiation in the narrow band because neither the ball or sapphire emissivity varies greatly from one band to the other. Consequently, the sapphire radiation will be neglected in the narrow band filter analysis as well.

The ambient radiation, like that from the ball, will be treated in the same manner as for the wide band except that fluid absorption is included. Equation (6) is therefore rewritten as equation (30).

$$\eta_o = \rho_s^* + \tau_s^{*2}\rho_b\tau_f(2h,T_f) \tag{30}$$

The transmissivity function is written here in terms of 2h since the ambient radiation must pass through the fluid film twice, a total

distance of 2h. (See Figure III-1.) The new transmissivity $\tau_f(2h)$ is not independent of $\tau_f(h)$ because both are given as explicit functions of h. To calculate values of $\tau_f(2h)$, 2h is substituted into equation (29) wherever the variable h appears.

Now that equations for attenuated radiation from the fluid, ball, and ambient have been derived, an equation can be formulated to give the total narrow band radiation in terms of the ball and fluid temperatures.

$$N = \tau_s^* \tau_f(h,T_f)\varepsilon_b N_{bb}(T_b) + \tau_s^* \varepsilon_f(h,T_f) N_{bb}(T_f) + [\rho_s^* + \tau_s^{*2} \rho_b \tau_f(2h,T_f)]N_o \quad (31)$$

Once the coefficients for $\varepsilon_f(h,T_f)$ and $\tau_f(h,T_f)$ have been determined through calibration, equation (31) can be solved for the fluid temperature by using either Figure III-4 (obtained through calibration) or equation (32) in an iteration scheme. Figure III-4 is the narrow band blackbody calibration curve and is analytically expressed as equation (32) by means of a least squares data fit.

$$N_{bb}(T) = Ae^{(c_1T^3 + c_2T^2 + c_3T + c_4)} \quad (32)$$

It should be apparent that in order to calculate the fluid temperature, the ball temperature must first be known. Because of this, a narrow band filter measurement is of no value unless accompanied by a wide band filter measurement to determine the ball temperature at the same location and under the same conditions.

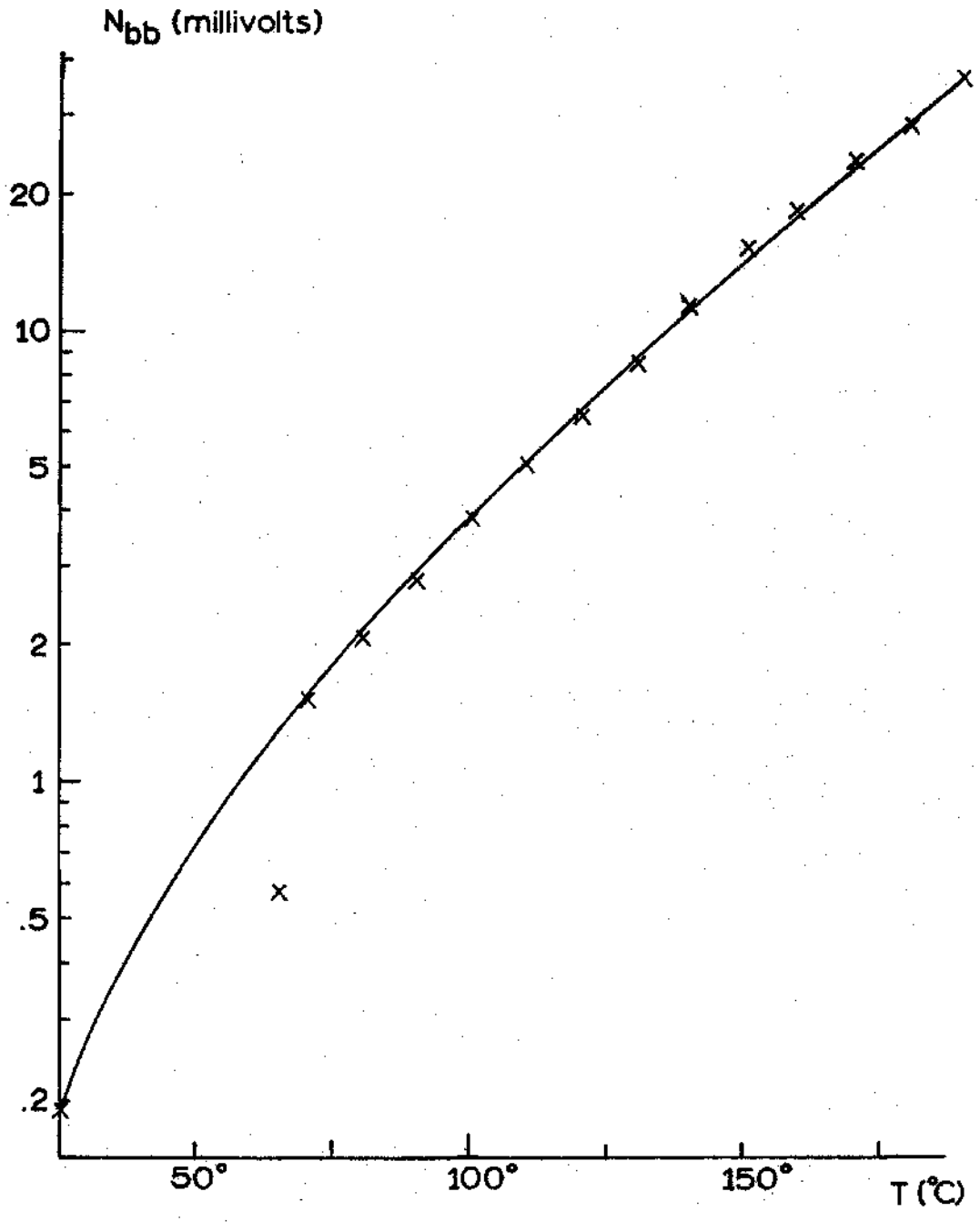

Figure III-4. Narrow Band Blackbody Calibration

At this point, a comparison of this technique with the earlier work [9, 10] is in order. Turchina's approach required that three measurements be taken at each location before solving for the ball surface and average lubricant temperatures. One measurement was taken with a standard ball (ε_b = .28) and another was taken using an oxide coated ball (ε_b = .53). No filter was used in either of these measurements. In addition, Turchina made a final measurement using a film of test lubricant as a filter to separate the lubricant contribution (N_f). The technique presented in this thesis is believed to be more accurate and thorough than Turchina's approach. Some of the improvements are listed below.

1. Turchina had to run three experiments for one set of data. Only two are required here and these can be combined into one by changing filters during the test run. Making fewer test runs minimizes any errors due to changing experimental conditions.

2. Prior to installation of the oil circulation system, lubricant inlet temperatures varied appreciably during test runs. This error has been eliminated here.

3. Turchina's analysis assumes that the fluid emissivity is independent of the ball reflectivity. This dependence is included here.

4. Turchina assumed that the lubricant emissivity and transmissivity varied linearly with film thickness. A more complete model is used here, but calibration results* indicate that the linear approximation is not a bad one.

---

*See Chapter IV.

CHAPTER IV

CALIBRATION

Blackbody Calibration

The Barnes Model RM-2A In-Sb Radiometric Microscope is accompanied by a blackbody calibration curve supplied by the manufacturer which shows the radiation intensity from a blackbody source as a function of the source temperature. However, the curve is not applicable when a filter is used and new calibration data must be experimentally obtained for each filter.

In order to calibrate for the filters, measurements of the radiation from a blackbody calibration source (Barnes Model RM-121) were taken using each filter. Although the calibration data are ultimately to be expressed as a plot of intensity versus source temperature, absolute measurements of the radiation intensity are not possible due to the nature of the equipment and the experimental technique. A single measurement of radiation through the filter can be expressed as follows:

$$N_a = N_{bb}(T) + N_{fil} - N_o' \tag{33}$$

In addition to radiation received from the blackbody source, $N_{bb}(T)$, an unknown quantity of radiation, N_{fil}, is emitted upward by the filter and collected by the detector. The quantity N_o' is a characteristic of the measurement system inside the detector and is known

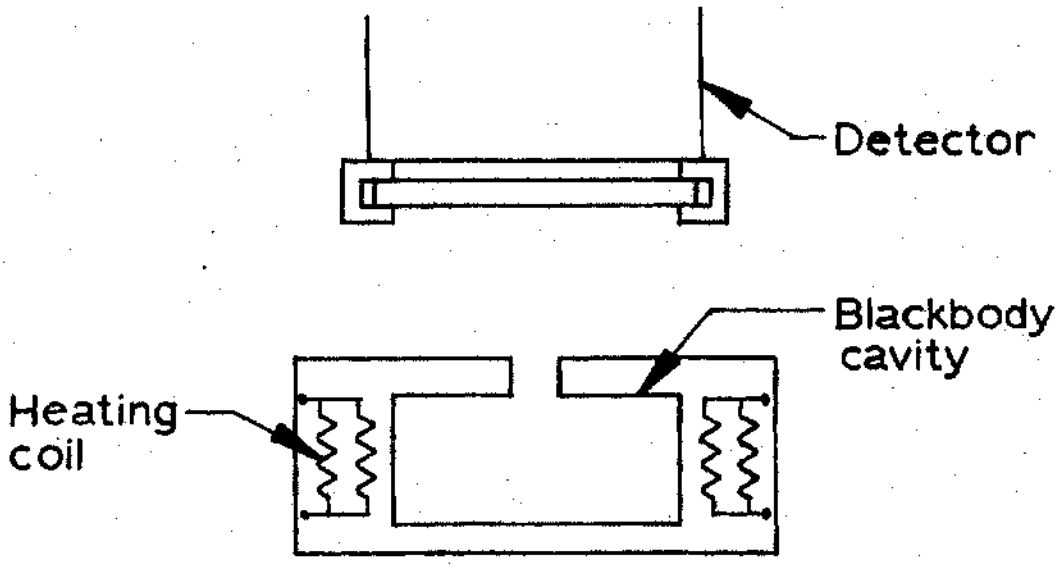

Figure IV-1. Blackbody Calibration Experiment

from calibration data supplied by the manufacturer. Because of the type of equipment used and the experimental technique employed, the actual measurement will not be that shown in equation (33), but rather the difference between it and the radiation measured from an ambient reference source at room temperature. The radiation from the ambient source is given in equation (34).

$$N_{a(amb)} = N_o + N_{fil} + N_o' \tag{34}$$

Therefore, the actual calibration measurement, N_m, is expressed by taking the difference of equations (33) and (34).

$$N_m = N_a - N_{a(amb)}$$

$$= N_{bb}(T) - N_o \tag{35}$$

At this point, the value of $N_{bb}(T)$ is still unknown because N_o is unknown. The variable N_o is the same one that was used in the wide and narrow band analyses and is equal to the intensity of radiation from a blackbody at room temperature.

$$N_o = N_{bb}(T_r) \tag{36}$$

Equation (36) is justified by the fact that the combined radiation emitted and reflected by an opaque surface at the same temperature as its surroundings will be the same as the radiation emitted by a blackbody at that temperature.

To determine N_o, a measurement was taken of a cryogenic blackbody source. The experiment was the same as shown in Figure IV-1, except that the manufacturer's blackbody source was replaced by a similar cavity immersed in a bath of liquid nitrogen (T = 77°K). The emission of a blackbody at 77°K in the infrared region can be shown by the Planck function to be less than 10^{-10} of the emission from a blackbody source at room temperature and can be neglected in the analysis. According to equation (35), the measured radiation is then equal to the negative of the ambient radiation. Once N_o is known, data in terms of $N_m(T)$ can be written in the form of $N_{bb}(T)$ and then plotted as a function of T. This technique was used to make Figures III-3 and III-4.

It should be mentioned here that all data obtained in this research are obtained in a similar manner; that is, they are referred to an ambient reference source and the values of N given in the main analysis will not be the actual measured values. Instead, they will

be the sum of both the measured and ambient values.

$$N_m = N - N_o$$

$$N = N_m + N_o \tag{37}$$

Calibration of the Lubricant Emissivity and Transmissivity

Before using equation (31) to calculate the fluid temperature, the lubricant's absorption and emission coefficients must be obtained through calibration. To determine these coefficients, radiation measurements were taken using a stationary contact where both the ball and fluid temperatures were known. In the calibration experiment, the same basic test apparatus is used but the ball is not rotated and there is no load on the contact. The film thickness at the contact center is zero and can be calculated at other locations by geometry.

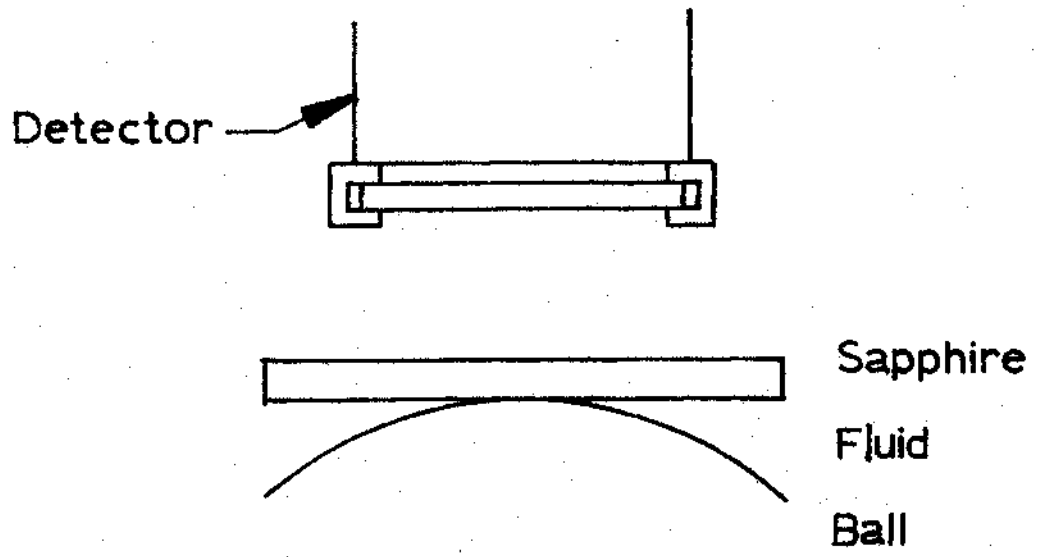

Figure IV-2. Lubricant Calibration Experiment

The circulating oil bath keeps the ball, oil, and sapphire all at the calibration temperature T_c. Under these conditions, a curve giving radiation as a function of film thickness is obtained as the detector transverses the contact.

When considering the radiation at the contact center (h = 0), the fluid neither emits nor absorbs and the calibration unknowns drop out of equation (31)

$$N(h=0) = \tau_s^* \varepsilon_b N_{bb}(T_c) + (\rho_s^* + \tau_s^{*2} \rho_b) N_o \tag{38}$$

Because T_c is known, the irradiance at h = 0 can be calculated. In the calibration experiment, a single traverse is made across the contact and the radiation is not referenced to ambient as in other experiments. This is done in the interest of obtaining greater amplification of the signal to help distinguish small variations in radiation at small film thicknesses. Instead of being referred to ambient, all data is referred to the intensity value at h = 0, which occurs as a minimum in the data photograph. The calibration data, now in the form $N(h) - N(h=0)$, are then fitted to a least squares third order function of film thickness.

$$N(h) - N(h=0) \approx N_1 h + N_2 h^2 + N_3 h^3 \tag{39}$$

If $T_f = T_b = T_c$, equation (31) can be written as follows:

$$N = \tau_s^* \tau_f(h,T_c) \varepsilon_b N_{bb}(T_c) + \tau_s^* \varepsilon_f(h,T_f) N_{bb}(T_c)$$

$$+ [\rho_s^* + \tau_s^{*2} \rho_b \tau_f(2h,T_c)] N_o \tag{40}$$

The oil emission and absorption coefficients are given in equations (21) and (29).

$$\varepsilon_f N_{bb}(T_f) = [(2 - \varepsilon_b)h\varepsilon_1(T_f) - (4 - 3\varepsilon_b)h^2\varepsilon_2(T_f) + (8 - 7\varepsilon_b)h^3\varepsilon_3(T_f)]N_{bb}(T_f) \quad (21)$$

$$\tau_f = 1 - [\alpha_1(T_f)h - \alpha_2(T_f)h^2 + \alpha_3(T_f)h^3] \quad (29)$$

Equations (21) and (29) can be substituted into equation (40), simplified, and rewritten in the form of equation (41).

$$N = [A\varepsilon_1(T_c) - D\alpha_1(T_c)]h + [-B\varepsilon_2(T_c) + E\alpha_2(T_c)]h^2 + [C\varepsilon_3(T_c) - F\alpha_3(T_c)]h^3 + \tau_s^*\varepsilon_b N_{bb}(T_c) + (\rho_s^* + \tau_s^{*2}\rho_b)N_o \quad (41)$$

The coefficients A, B, C, D, E, anf F are defined by equations (42a) through (42f).

$$A = \tau_s^*(2 - \varepsilon_b)N_{bb}(T_c) \quad (42a)$$

$$B = \tau_s^*(4 - 3\varepsilon_b)N_{bb}(T_c) \quad (42b)$$

$$C = \tau_s^*(8 - 7\varepsilon_b)N_{bb}(T_c) \quad (42c)$$

$$D = \tau_s^*\varepsilon_b N_{bb}(T_c) + 2\tau_s^{*2}\rho_b N_o \quad (42d)$$

$$E = \tau_s^*\varepsilon_b N_{bb}(T_c) + 4\tau_s^{*2}\rho_b N_o \quad (42e)$$

$$F = \tau_s^* \varepsilon_b N_{bb}(T_c) + 8\tau_s^{*2} \rho_b N_o \tag{42f}$$

Subtracting equation (38) from equation (41), equation (43) is obtained.

$$N - N(h=0) = [A\varepsilon_1(T_c) - D\alpha_1(T_c)]h + [-B\varepsilon_2(T_c) + E\alpha_2(T_c)]h^2 + [C\varepsilon_3(T_c) - F\alpha_3(T_c)]h^3 \tag{43}$$

Combining equation (43) with equation (39) and equating coefficients for each power of h results in three separate equations.

$$A\varepsilon_1(T_c) - D\alpha_1(T_c) = N_1 \tag{44a}$$

$$-B\varepsilon_2(T_c) + E\alpha_2(T_c) = N_2 \tag{44b}$$

$$C\varepsilon_3(T_c) - F\alpha_3(T_c) = N_3 \tag{44c}$$

The above equations each contain two unknowns and therefore cannot be solved by using the data from a single calibration experiment. To find another set of equations, another calibration experiment is performed at the same temperature but using a ball with a different emissivity. Then using the same procedure as above, a second set of equations is obtained in the same fashion as equations (44).

$$A'\varepsilon_1(T_c) - D'\alpha_1(T_c) = N_1 \tag{45a}$$

$$-B'\varepsilon_2(T_c) + E'\alpha_2(T_c) = N_2 \tag{45b}$$

$$C'\epsilon_3(T_c) - F'\alpha_3(T_c) = N_3 \qquad (45c)$$

Equations (44a) and (45a) both contain the calibration unknowns ϵ_1 and α_1, and can be solved simultaneously for these two variables. Likewise, equations (44b) and (45b) can be solved for ϵ_2 and α_2, and equations (44c) and (45c) can be solved for ϵ_3 and α_3. Solving for these six coefficients will then provide complete functions of both the lubricant's emissivity and its transmissivity for grey and blackbody radiation at the calibration temperature.

Figure IV-3 shows the results that were obtained when the test lubricant was calibrated at 100°C using this technique. In the experiment, data were taken using both the standard chrome steel ball ($\epsilon_b = 0.28$) and a ball coated with a metallic oxide ($\epsilon_b = 0.53$). Another set of data was taken using a similar ball plated with a silver coating ($\epsilon_b = 0.07$) to verify the results. Substituting data from the silver ball for either the standard or the oxide coated ball was found to have no appreciable effect on the final emissivity and transmissivity functions obtained.

To this point, no attempt has been made to calibrate the lubricant as a function of temperature. The calibration results shown in Figure IV-3 are good only at 100°C and would not be expected to be applicable at other temperatures. This problem is increased by a lack of information in the literature concerning emissive and transmissive properties of typical lubricants, particularly with respect to temperature. Therefore, the only way to apply this technique is to calibrate at several temperatures and develop relationships for both emissivity and transmissivity with temperature.

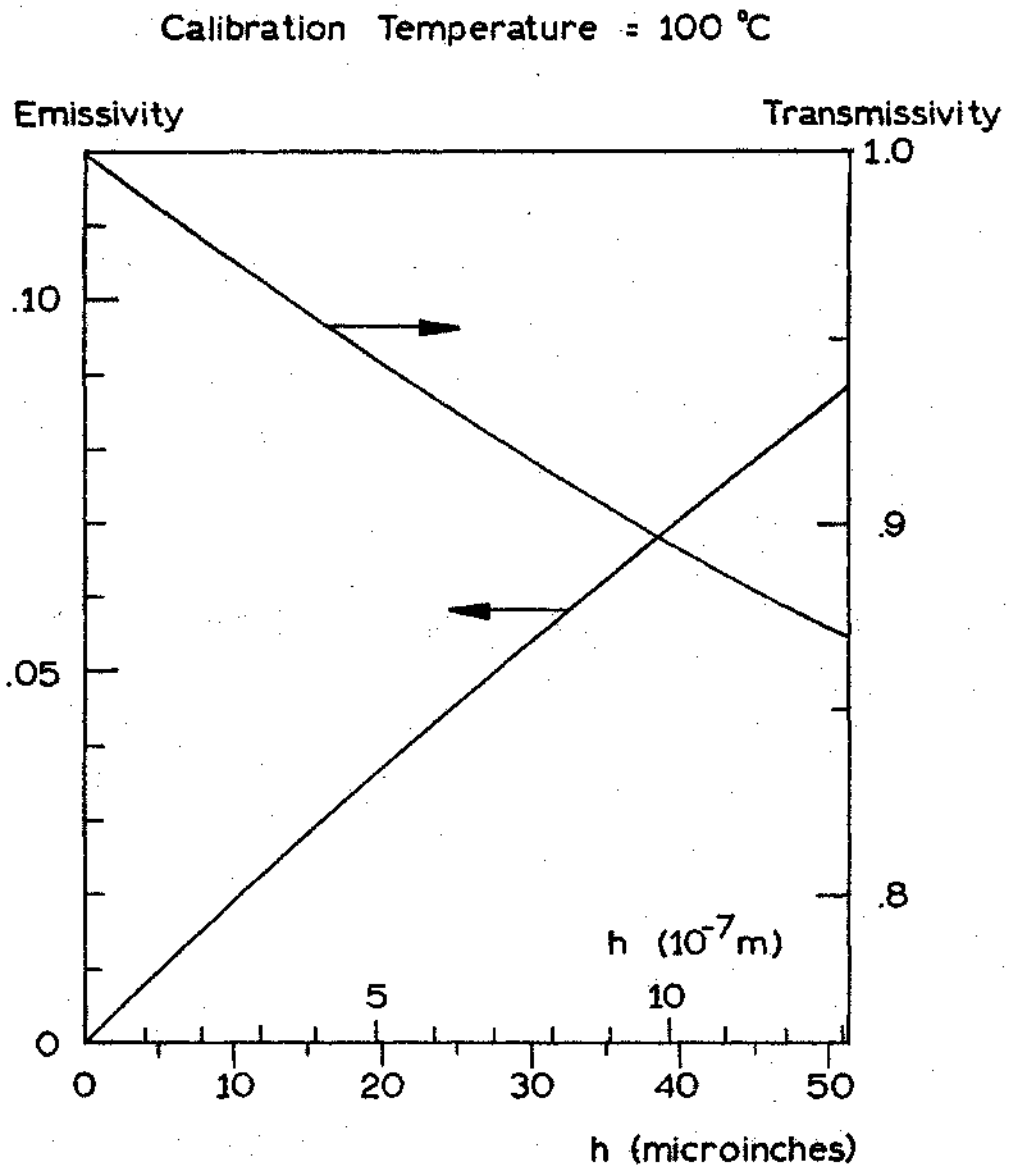

Figure IV-3. Emissivity and Transmissivity versus Film Thickness

To solve for the temperatures which are presented in Chapter V, the calibration technique was applied at several temperatures to obtain curves similar to Figure IV-3. After considering data taken between 70°C and 120°C, the following equations for emissivity and transmissivity were used to give an approximation to the data over the range of calibration temperatures.

$$\varepsilon_f = 1 - e^{-A_1 h e^{B_1 T_f}} \tag{46}$$

$$\tau_f = e^{-A_2 h e^{B_2 T_f}} \tag{47}$$

CHAPTER V

EXPERIMENTAL RESULTS

This technique was used to determine ball surface and average lubricant temperatures at a number of sliding speeds.* In this research the same experimental apparatus and the same test lubricant that has already been described was utilized. The load for all tests was kept constant at 67 N (15 lbf) which corresponds to a maximum theoretical Hertzian pressure of 1.04×10^9 N/m^2. The sliding speed was varied from 0.348 m/sec to 2.54 m/sec. The contact feed reservoir oil temperature was maintained at 40°C.

Ball surface temperatures were calculated by solving equations (8) and (9) for T_b at locations spaced 2.54×10^{-5} m (.001 in) apart in the contact. One set of results, taken at a sliding speed of 1.40 m/sec, is illustrated in Figure V-1 as a map showing isothermals at 10°C intervals. The results are only given for half of the contact based on the assumption that temperatures in the other half will be identical due to symmetry.

Figure V-2 shows the average lubricant temperatures calculated from data taken under the same conditions. The temperatures were calculated by considering the ball surface temperatures shown in Figure V-1 along with film thickness data for the same lubricant at

---

*Most of the actual experimental work presented here was done by H. S. Nagaraj.

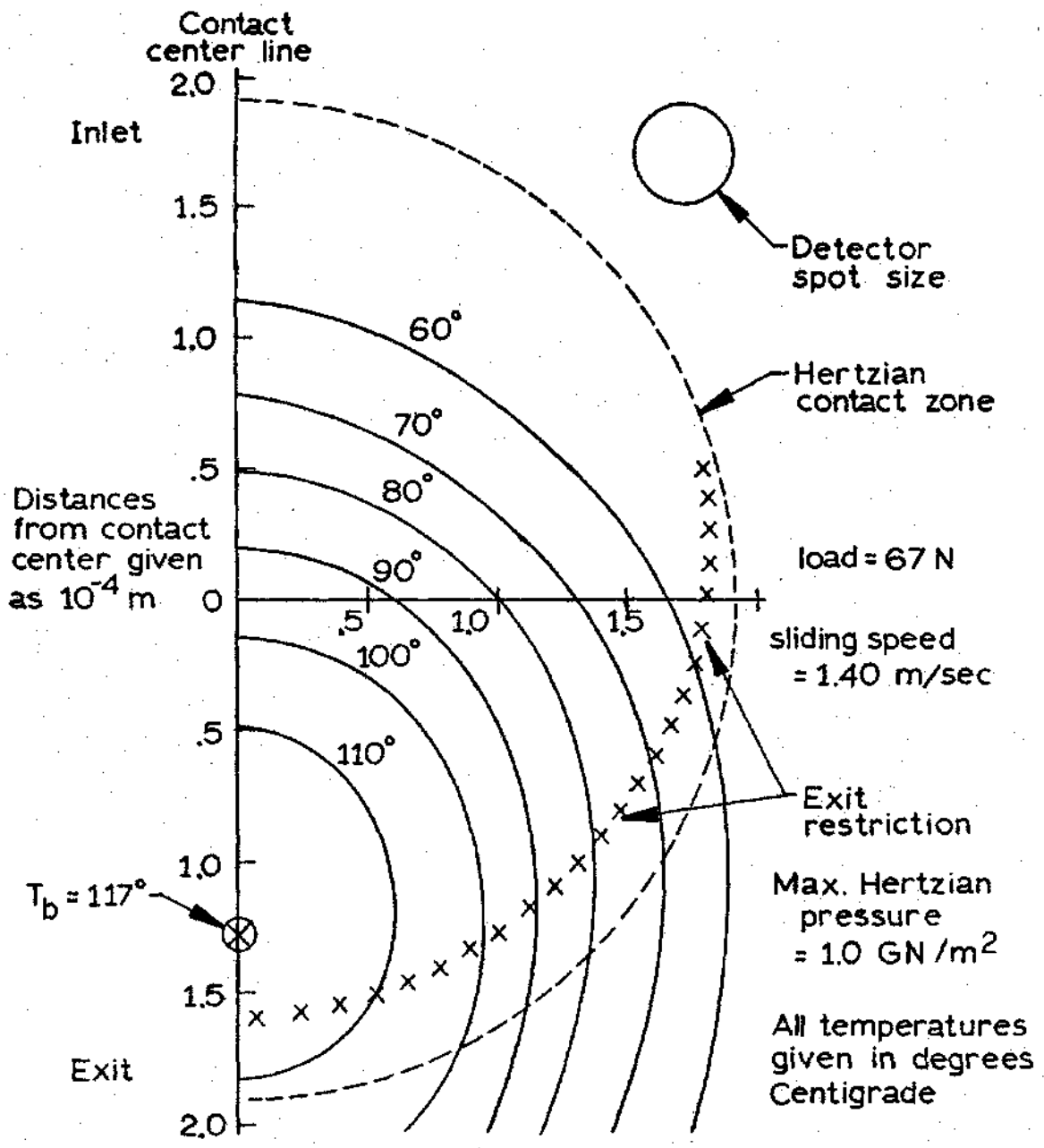

Figure V-1. Ball Surface Temperature

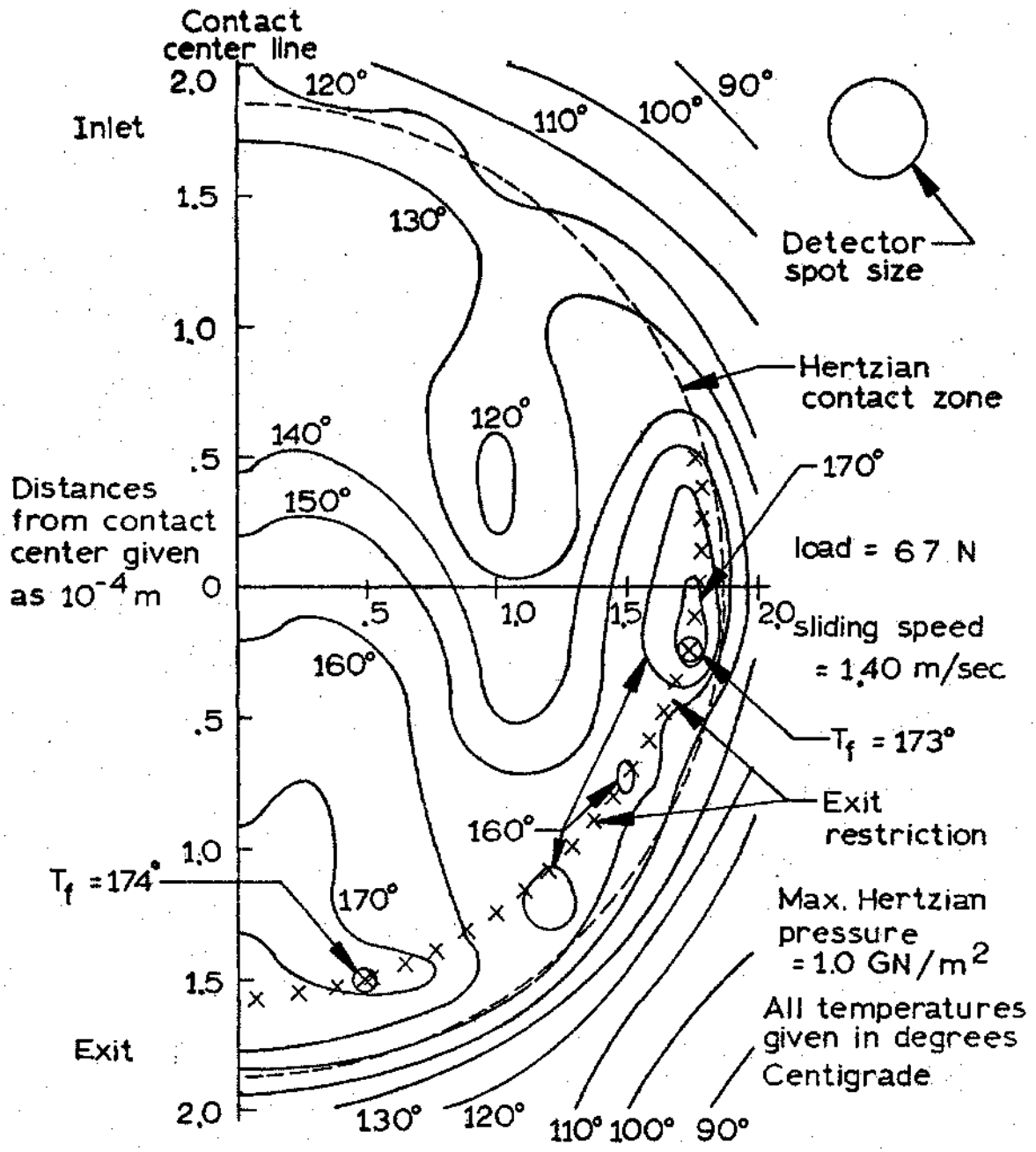

Figure V-2. Average Lubricant Temperature

1.40 m/sec taken in another experiment.

The film thickness measurements were made with the same test rig using the optical interference technique described by Sanborn and Winer [2]. Regions of low film thickness have been shown in both figures. These regions occur wherever oil is leaving the Hertzian contact zone and form a distinctive horseshoe shape. This pattern is characteristic of EHD sliding point contacts and the low film thickness regions are known as the exit restriction. With the exception of the exit restriction, film thickness remains virtually constant throughout the contact zone.

The ball surface reaches its maximum temperature along the contact center line. The maximum temperature is 117°C and occurs 1.3×10^{-4} m (.005 in) behind the contact center, or approximately 5×10^{-5} m (.002 in) before the exit restriction. Both the shape of the contours and the location of the maximum indicate that the ball is heated primarily by conduction from the oil. Along the center line, the ball is in contact with hot oil for a longer period of time and consequently reaches a higher temperature. It is interesting to note that the ball temperature remains low in the side lobes, where the minimum film thickness occurs. The side lobe restriction has a film thickness of only 5×10^{-8} m (two microinches), and there would seem to be a great probability of asperity contact in this region since both the ball and the sapphire have surface roughnesses of approximately 2.5×10^{-8} m (one microinch). However, any metal-to-sapphire contact, in all likelihood, would cause an increase in the ball surface temperature in the side lobes. The absence of any such temperature increase

would then tend to substantiate Fowles' theory [3] which suggests that individual asperity-asperity interactions occur without actual surface-to-surface contact.

The highest oil film temperatures, not surprisingly, are encountered in the low film thickness regions. Temperatures over 170°C are found both in the side lobes and in the center toward the rear of the contact zone. In the exit restriction, the oil temperature never goes below 150°C. As would be expected, the highest temperature gradient is located in the side lobes. In fact, the lubricant's average temperature increases by more than 20°C while it travels a distance of 2.5×10^{-8} m (one microinch) through the side lobes.

Although the oil bath temperature was only 40°C, there were no measured temperatures below 75°C and the oil entering the contact had already been heated to over 120°C in most cases. Therefore, the oil is heated more than 80°C before entering the contact, but no more than 60°C while going through it. A typical oil film generated at this sliding speed is subjected to an average shear rate of about 1×10^{7} sec^{-1} and the energy added to the oil on a per unit volume basis is orders of magnitude higher inside the contact than outside of it. This relatively small temperature increase would indicate that large quantities of heat are removed from the oil by conduction to the ball surface and that convection plays only a minor role in cooling. Some energy could also be dissipated by molecular degradation of the lubricant.

Figure V-3 shows the lubricant and ball surface temperatures and the film thickness along the contact center line for the same

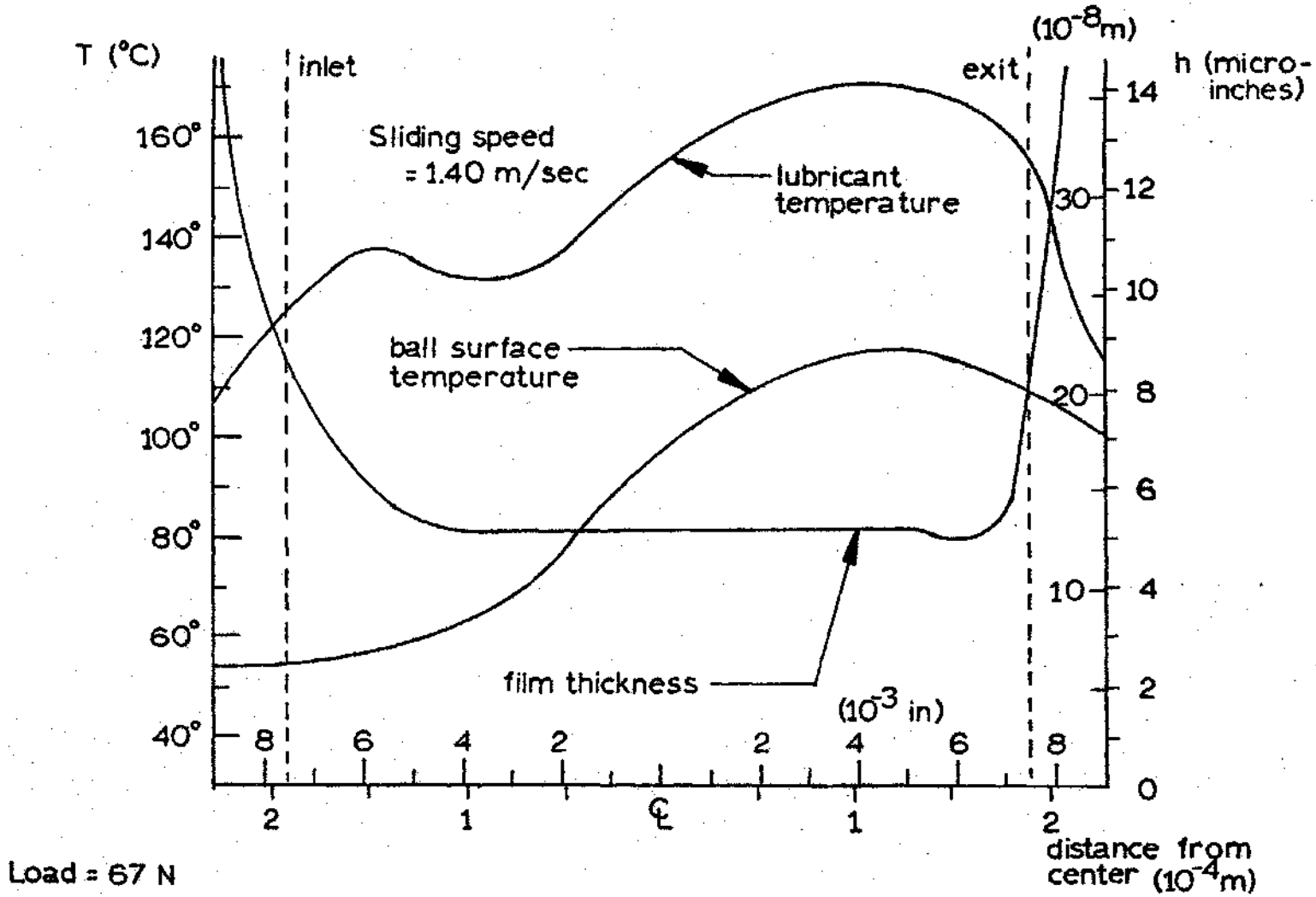

Figure V-3. Lubricant and Ball Surface Temperatures Along Contact Center Line

sliding speed. The ball surface exhibits a rapid increase in temperature once it reaches the contact zone, reaches a maximum toward the end of the contact, and begins to decrease shortly after the oil film temperature begins to decrease. The behavior of the lubricant is somewhat more difficult to describe. Shortly after entering the contact, the oil actually decreases in temperature.

The ball surface temperature distribution shown in Figure V-1 is representative of those observed at all sliding speeds except for magnitude. In all cases, the maximum temperature is found along the center line toward the rear of the contact. There was also no evidence of any surface-to-surface contact at any of the sliding speeds. Even at 13.7 ips, where film thicknesses were lowest, there was no ball surface temperature increase that would have distinguished the side lobes. The maximum ball surface temperature has been plotted as a function of sliding speed in Figure V-4. The resulting curve shows a continuous increase in temperature with increasing sliding speed, but the rate of increase slows considerably at higher speeds.

The maximum lubricant temperature, the lubricant temperature at the contact center, the contact center film thickness, and the minimum film thickness have also been plotted in Figure V-4. At all speeds, the maximum temperature occurred somewhere along the exit restriction. When the maximum temperature is compared to sliding speed, it is found to reach a minimum between 1.3 and 2.0 m/sec (50 and 80 ips). The low sliding speeds, because of their low film thicknesses, increased the likelihood of asperity interactions and also caused the energy from mechanical shearing to be distributed

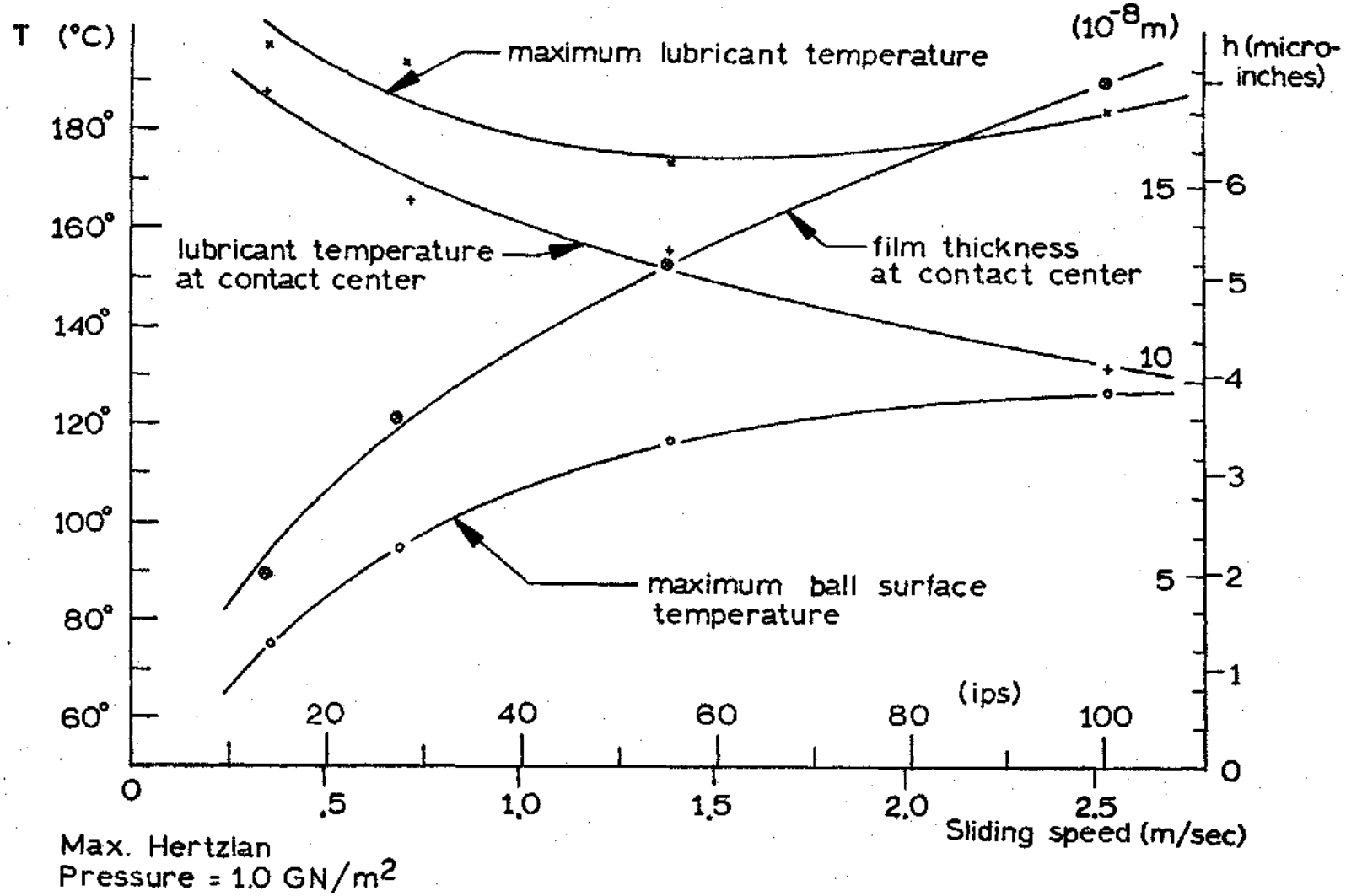

Figure V-4. Temperature and Film Thickness versus Sliding Speed

through a much thinner film. Higher sliding speeds, on the other hand, increased the total energy added to the lubricant and also caused higher temperatures.

The oil temperature at the contact center behaves differently as a function of sliding speed. The temperature there, which is more representative of temperatures in most of the contact zone, steadily decreases with higher sliding speeds, apparently because of higher film thicknesses. This does not mean, however, that higher sliding speeds are necessarily desirable. Due to the fact that the highest oil temperatures are always found at locations of minimum film thickness, the maximum lubricant temperature, as plotted in Figure V-4, could signal some form of film breakdown. Assuming that bearing surface wear will occur at these locations, the sliding speeds which yield the lowest maximum temperatures should be the best in terms of preventing wear. A bearing designer who would be subject to the same constraints as were found in this experiment might try to operate at a sliding speed of between 1.3 and 2.0 m/sec (50 and 80 ips) to minimize wear, preferably closer to 1.3 m/sec to minimize friction.

CHAPTER VI

CONCLUSIONS

The research presented here demonstrates the effectiveness of applying infrared scanning to bearing temperature analysis. Irradiances obtained by measuring at several locations in the contact through two different IR filters have been analyzed to calculate the radiation intensities from the ball surface and from the lubricant. Temperatures for the ball surface and lubricant were then calculated by considering the emissive and transmissive properties of the various bodies and media.

To help show the technique's usefulness, a set of temperature data obtained using this technique has been included in Chapter V. The temperature data was taken at 66.7 N at sliding speeds varying from 0.348 to 2.54 m/sec. The data showed that the ball reached temperatures as high as 127°C, and the lubricant reached temperatures as high as 197°C in the range of sliding speeds.

IR temperature mapping has a considerable amount of potential for applications in EHD sliding point contacts. This research has already shown some of the effects on temperature that are evident with changes in sliding speed. In the future, similar data could also be taken to study the effects of load, bearing surface roughness, and lubricant viscosity, among other things. Such data should be useful in formulating a better understanding of lubricant and bearing behavior under extreme operating conditions.

REFERENCES

1. Dowson, D. and Higginson, G. R., Elastohydrodynamic Lubrication, London, 1966.

2. Sanborn, D. M. and Winer, W. O., "Fluid Rheological Effects in Sliding Elastohydrodynamic Point Contacts with Transient Loading: I: Film Thickness," Journal of Lubrication Technology, ASME Transactions, Series F, Vol. 93, No. 2, April 1971, p. 262.

3. Fowles, P. E., "A Thermal Elastohydrodynamic Theory for Individual Asperity-Asperity Collisions," Journal of Lubrication Technology, ASME Transactions, Series F, Vol. 93, No. 3, July 1971, p. 383.

4. Cheng, H. S. and Sternlicht, B., "A Numerical Solution for the Pressure, Temperature, and Film Thickness Between Two Infinitely Long, Lubricated Rolling and Sliding Cylinders, Under Heavy Loads," Journal of Basic Engineering, ASME Transactions, Vol. 87, 1965, p. 695.

5. Crook, A. W., "The Lubrication of Rollers--III," Philosophical Transactions of the Royal Society, Vol. 255, 1963, p. 281.

6. Dowson, D. and Higginson, G. R., "A Numerical Solution to the Elastohydrodynamic Problem," Journal of Mechanical Engineering Science, Vol. 1, No. 1, 1959, p. 6.

7. Jakobsen, J., Lubricant Rheology at High Shear Stress, unpublished doctoral thesis, Georgia Institute of Technology, September 1973.

8. Walker, D., Sanborn, D. M., and Winer, W. O., "Molecular Degradation of Lubricants in Sliding Elastrohydrodynamic Contacts," to appear in Journal of Lubrication Technology, ASME Transactions, Series F, Paper No. 74-Lub-35, 1974.

9. Turchina, V. A., Pressure and Temperature Measurement Techniques in Elastohydrodynamic Contacts, unpublished master's thesis, Georgia Institute of Technology, June 1973.

10. Turchina, V. A., Sanborn, D. M., and Winer, W. O., "Temperature Measurements in Sliding Elastohydrodynamic Point Contacts," Journal of Lubrication Technology, MAME Transactions, Vol. 96, July 1974, p. 464.

11. Sanborn, D. M. and Winer, W. O., "Fluid Rheological Effects in Sliding Elastohydrodynamic Point Contacts with Transient Loading:

II: Traction," Journal of Lubrication Technology, ASME Transactions, Series F, Vol. 93, No. 3, July 1971, p. 342.

12. Siegel, R. and Howell, J. R., Thermal Radiation Heat Transfer: III: Radiation Transfer with Absorbing, Emitting, and Scattering Media, NASA SP-164.

13. Kreith, F., Principles of Heat Transfer, International Textbook Company, 1964.

14. Nagaraj, H. S., Carlson, S., Molina-Combita, Sanborn, D. M., and Winer, W. O., "Investigations of Lubricant Theology at High Shear Stress," NASA Grant No. 11-002-133, CR-134730, September 1974, p. 29.